A Compact Tri-Band Impedance-Transforming Power Divider With Independent Controllable Power Division Ratios and Enhanced Bandwidths

YUHAO YANG[1], NAN HU[2], (Senior Member, IEEE), WENQING XIE[2],
WEIMIN WANG [1], AND YONGLE WU [1], (Senior Member, IEEE)

[1]Beijing Key Laboratory of Work Safety Intelligent Monitoring, School of Electronic Engineering, Beijing University of Posts and Telecommunications, Beijing 100876, China
[2]A-INFO Inc., Beijing 100084, China

Corresponding author: Yongle Wu (wuyongle138@gmail.com)

ABSTRACT In this paper, a tri-band impedance transformer (TBIT) using a coupled line and a dual-band to tri-band transformer is proposed, which can transform frequency-dependent complex impedances to a real-value impedance. In order to explain how to determine circuit parameters, closed-form equations are derived in detail. Based on the TBIT, a compact T-junction power divider (TTPD) is designed. This TTPD works at three different frequencies with independent controllable power division ratios. Simple steps to design the TTPD are listed. To demonstrate the validity of the theory, this paper exhibits a prototype operating at 2, 4.4, and 5 GHz with different power division ratios. Moreover, the simulated and measured results prove that this TTPD has the features of tri-band operation, independent controllable power division ratios, enhanced bandwidths, and small size.

INDEX TERMS Independent controllable power division ratios, tri-band, impedance transformer, power divider.

I. INTRODUCTION

In the future, a few mobile communication systems including 2G to 5G will run simultaneously, however, the frequencies their services use are not constant. Different operation frequencies demand multi-band operation microwave components. Researches on how to expand components' operation bandwidths and design multi-band operation microwave components, have received many attentions payed by designers.

Wideband power dividers (PD) become more popular in recent years [1], but it's not enough for PDs to operate in a single band. Therefore, a varactor based frequency-tunable power divider is created [2], by inserting some varactors into the circuit, its operation band can cover 0.85-2.4 GHz. Nevertheless, the tuning method is so inconvenient.

The associate editor coordinating the review of this manuscript and approving it for publication was M. Jahangir Hossain.

To invent multi-band PDs, designers begin to improve conventional PDs such as Wilkinson Power Dividers and Gysel Power Dividers. Multi-section transmission lines are used to replace $\lambda/4$ transmission lines in Wilkinson Power Dividers [3]. Many transmission lines and stub lines can make up dual-band PDs together [4], [5], obviously calculations become complex due to the extra circuit structures. Some designs use $\lambda/4$ open stubs to introduce transmission zeros to isolate operation frequencies [6]–[8]. But there is a disadvantage that additional open stubs enlarge the size. Because coupled lines are good for reducing the size of the circuit, they become common in PDs [9]–[18]. At the same time, there is a significate trend that PDs provide more and more functions such as unequal power dividing, out-phase output, filtering, and impedance transforming. In order to realize these functions, more technologies are fused into PDs' designs. Bandpass filters are added into the design in [19]. A phase inverter which can reduce the circumference of Gysel Power Divider and improve the bandwidth, becomes a part of

the PD mentioned in [20]. Resonators have been involved in PDs [21]–[24]. However, the PDs including resonators have narrow bandwidths and complicated structures. Since using conventional transmission lines to design PDs is short of innovation, improved transmission lines such as non-uniform transmission lines and composite right- and left-handed transmission lines play important roles in PDs [25], [26]. In addition, some out-of-phase PDs with high frequency ratios can be widely used in many applications [27], [28].

In recent years, the development on PDs mainly focuses on dual-band PDs. Tri-band PDs are rare yet. As we all know, electrical lengths of transmission lines and coupled lines are related to frequencies, so the introduction of any line has an impact on the circuit parameters at three operation frequencies and it is hard to find out an appropriate method to make sure that designs have excellent performances at three frequencies simultaneously. In order to satisfy the conditions of tri-band operation, designers have no choice but to make their designs have more changeable circuit parameters, but complexity increases [5]–[7], [29]. Two approaches to design multi-band PDs are summarized in [30] and a similar design idea is shown in [31]. However, the functions that tri-band PDs have are less than dual-band PDs have, so there is huge development space for tri-band PDs.

The impedance transformer has become a part of the design in [30]. As we all know, characteristic impedances and electrical lengths of transmission lines can be modified in the fabrication process, so the use of transmission lines makes impedance transformation controllable. Two-section transmission lines are used to realize dual-band impedance transformers [32], [33]. Other dual-band impedance transformers with different structures are shown in [34]–[37]. However, they can't be used in tri-band applications. The design in [38] uses stubbed coupled lines to design a tri-band transformer with a small size, but it has a limitation on operation frequencies. In [39], the complex structure of the multi-frequency impedance transformer makes the integration low. A new concept of impedance matching using a common reference frequency is proposed in [40] and [41], in my opinion, this concept is strict with load impedances and a little change on load impedances may bring a big influence. As the result, designs in [40] and [41] have narrow bandwidths. Another impedance matching network mentioned in [42] can only realize transformation between two real-value impedances. The tri-band impedance transformer used in this paper can transform frequency-dependent complex impedances to a real-value impedance.

For making tri-band PDs better, this paper does some significant jobs. A TBIT is introduced in this paper and it uses a coupled line to enhance the bandwidth and reduce the size. According to the method to design T-junction PDs [29], a simple way to obtain controllable division ratios is introduced in this paper. Finally, this paper proposes a TTPD with independent controllable power division ratios and enhanced bandwidths. Compared to the TTPD in [29], this TTPD has wider bandwidths and a smaller size. The 3D structure of
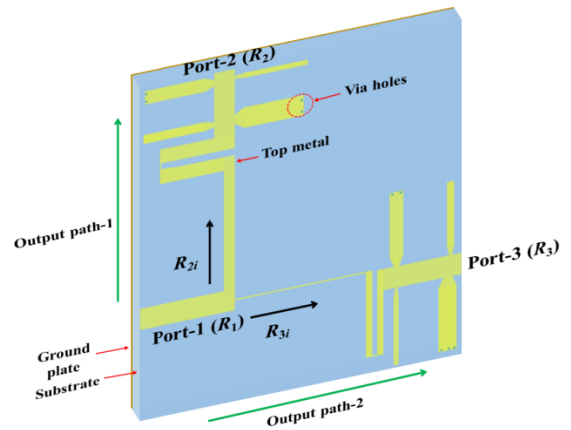

FIGURE 1. The 3D structure of the tri-band T-junction power divider.

this power divider is shown in Fig. 1. The circuit analysis explains how circuit parameters influence operation frequencies and power division ratios. A TTPD operating at the center frequencies of 2.0 GHz, 4.4 GHz, and 5.0 GHz is simulated. The reason why this design chooses 2.0 GHz, 4.4 GHz and 5.0 GHz as operation frequencies is that the band near 2.0 GHz is used by 4G mobile communication system and the band covering 4.4 GHz to 5.0 GHz is likely to be used by 5G. The power division ratios at these three different frequencies are -4.44 dB, 0.00 dB, and -3.10 dB. The corresponding printed circuit board (PCB) is fabricated on the RO4350B substrate. There is a good agreement between simulated results and measured results.

II. THEORY AND DESIGN

The proposed TTPD is improved from the conventional T-junction power divider. The 3D structure is shown in Fig. 1. Two TBITs are located between the input port and two output ports.

A. TRI-BAND IMPEDANCE TRANSFORMER

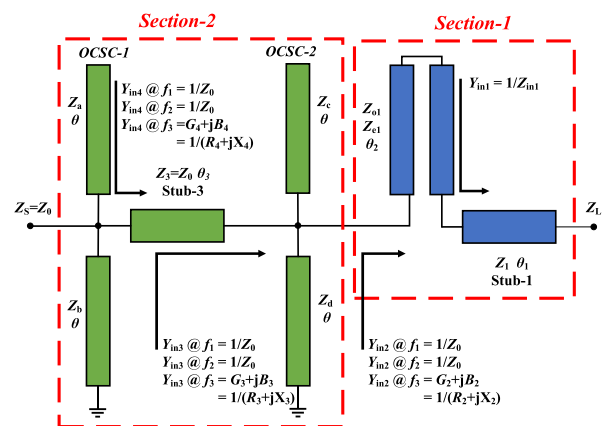As is depicted in Fig. 2, the TBIT consists of two sections, one is a dual-band impedance transformer which uses a

FIGURE 2. The circuit structure of the tri-band impedance transformer.

coupled line and a transmission line, the other is a dual-band to tri-band transformer using open-circuited-short-circuited (OCSC) stubs. Section-1 changes frequency-dependent complex load impedances at f_1 and f_2 to Z_0 which is equal to Z_3 and Z_S, section-2 changes the impedance at f_3 to Z_0 without influencing the impedance matching at f_1 and f_2.

The first part of the TBIT is a dual-band impedance transformer. This part includes a cascaded transmission line and a coupled line. By using the coupled-line theory and the common even-odd model method, the ABCD matrix of this coupled line can be calculated [37], [43]. Parameters included in the matrix are expressed as

$$
\begin{bmatrix} A & B \\ C & D \end{bmatrix} = \begin{bmatrix} \dfrac{Z_e - Z_o \tan^2(\theta_2)}{Z_e + Z_o \tan^2(\theta_2)} & \dfrac{2jZ_eZ_o \tan(\theta_2)}{Z_e + Z_o \tan^2(\theta_2)} \\ \dfrac{2j \tan(\theta_2)}{Z_e + Z_o \tan^2(\theta_2)} & \dfrac{Z_e - Z_o \tan^2(\theta_2)}{Z_e + Z_o \tan^2(\theta_2)} \end{bmatrix},
$$
(1)

Z_o and Z_e are the odd- and even-mode impedance, θ_2 is the electrical length of the coupled line. And any electrical length shown in Fig. 2 is defined at f_1.

The coupled line transforms Y_{in1} to Y_{in2}. There is an equation to make sure that Y_{in2} is equal to $1/Z_0$ at f_1 and f_2. This equation is the key of the following discussion

$$
Z_0 = \frac{A|_{f_1} * Z_{in1}|_{f_1} + B|_{f_1}}{C|_{f_1} * Z_{in1}|_{f_1} + D|_{f_1}} = \frac{A|_{f_2} * Z_{in1}|_{f_2} + B|_{f_2}}{C|_{f_2} * Z_{in1}|_{f_2} + D|_{f_2}},
$$
(2)

where Z_{in1} can be expressed as

$$
Z_{in1} = R_1 + jX_1 = \frac{1}{Y_{in1}}.
$$
(3)

Obviously, tunable parameters included in (1) and (2) are Z_o, Z_e, and θ_2, but they are not enough to make Y_{in1} @ f_1 and Y_{in1} @ f_2 be transformed to $1/Z_0$ simultaneously. If Z_{in1} @ f_1 is the complex conjugate impedance of Z_{in1} @ f_2, the tuning process of Z_o, Z_e, and θ_2 will be easy. In order to do this, a cascaded transmission line is placed on the right of the coupled line. The analysis in [37] confirms that when Z_1 and θ_1 are determined by (4)-(5), R_1 @ $f_1 = R_1$ @ f_2 and X_1 @ $f_1 = -X_1$ @ f_2

$$
Z_1 = \sqrt{\begin{array}{c} R_L|_{f_1} R_L|_{f_2} + X_L|_{f_1} X_L|_{f_2} \\ + \dfrac{\left(X_L|_{f_1} + X_L|_{f_2}\right)\left(R_L|_{f_1} X_L|_{f_2} - X_L|_{f_1} R_L|_{f_2}\right)}{R_L|_{f_2} - R_L|_{f_1}} \end{array}},
$$
(4)

$$
\theta_1 = \frac{n\pi + \arctan\left[\dfrac{Z_1\left(R_L|_{f_1} - R_L|_{f_2}\right)}{R_L|_{f_1} X_L|_{f_2} - X_L|_{f_1} R_L|_{f_2}}\right]}{1 + u_1},
$$
(5)

where n is a natural number. Once Z_1 and θ_1 are known, R_1 @ f_1 and X_1 @ f_1 can be written as

$$
R_1|_{f_1} = \frac{Z_1^2 R_L|_{f_1}\left(1 + \tan^2(\theta_1)\right)}{\left[Z_1 - X_L|_{f_1}\tan(\theta_1)\right]^2 + R_L^2|_{f_1}\tan^2(\theta_1)},
$$
(6)

$$
X_1|_{f_1} = \frac{Z_1\left[\begin{array}{c} Z_1 X_L|_{f_1} - Z_1 X_L|_{f_1}\tan^2(\theta_1) \\ + \left(Z_1^2 - R_L^2|_{f_1} - X_L^2|_{f_1}\right)\tan(\theta_1) \end{array}\right]}{\left[Z_1 - X_L|_{f_1}\tan(\theta_1)\right]^2 + R_L^2|_{f_1}\tan^2(\theta_1)}.
$$
(7)

The condition that Z_{in1} @ f_1 and Z_{in1} @ f_2 are complex conjugate impedances makes the simplification of (2) possible. (8) can be derived from (2)

$$
\begin{aligned} 2X_1|_{f_1} Z_0 \tan(\theta_2) \\ = \left(Z_0 - R_1|_{f_1}\right)\left[Z_e - Z_o \tan^2(\theta_2)\right], \end{aligned}
$$
(8a)

$$
\begin{aligned} 2\left(R_1|_{f_1} Z_0 - Z_eZ_o\right)\tan(\theta_2) \\ = X_1|_{f_1}\left[Z_e - Z_o \tan^2(\theta_2)\right], \end{aligned}
$$
(8b)

$$
\begin{aligned} -2X_1|_{f_2} Z_0 \tan(u_1\theta_2) \\ = \left(Z_0 - R_1|_{f_1}\right)\left[Z_e - Z_o \tan^2(u_1\theta_2)\right], \end{aligned}
$$
(8c)

$$
\begin{aligned} 2\left(R_1|_{f_1} Z_0 - Z_eZ_o\right)\tan(u_1\theta_2) \\ = -X_1|_{f_1}\left[Z_e - Z_o \tan^2(u_1\theta_2)\right], \end{aligned}
$$
(8d)

where $u_1 = f_2/f_1$. Solving (8a) and (8b) can obtain expressions of the odd- and even-mode impedance of the coupled line. The expressions are (9) and (10), as shown at the bottom of this page.

By comparing (8b) and (8d), there is a discovery that (11) can make (8b) and (8d) have solutions at the same time. Herein, m refers to a positive integer

$$
\theta_2 = \frac{m\pi}{1 + u_1}.
$$
(11)

For Y_{in2} at f_3, when the changeable parameters of section-1 are all clear, it can be got by a few simple mathematical calculations by (1), (2), (6), and (7). Parameters at f_1 in these formulas must be replaced by parameters at f_3.

The premise of section-2's design is that it transforms Y_{in2} at f_3 to $1/Z_0$ without influencing the already obtained impedance matching at f_1 and f_2. The first thing is discussing how OCSC stubs avoid affecting the impedance matching

$$
Z_o = \frac{-\dfrac{2X_1|_{f_1} Z_0 \tan(\theta_2)}{(Z_0 - R_1|_{f_1})} \pm \sqrt{\left[\dfrac{2X_1|_{f_1} Z_0 \tan(\theta_2)}{(Z_0 - R_1|_{f_1})}\right]^2 - 4\tan^2(\theta_2)\left[\dfrac{X_1^2|_{f_1} Z_0}{Z_0 - R_1|_{f_1}} - R_1|_{f_1} Z_0\right]}}{2\tan^2(\theta_2)},
$$
(9)

$$
Z_e = \frac{2X_1|_{f_1} Z_0 \tan(\theta_2)}{(Z_0 - R_1|_{f_1})} + Z_o \tan^2(\theta_2),
$$
(10)

at f_1 and f_2 [42]. The combined admittance generated by OCSC-1 is written as

$$Y_{OCSC} = j\frac{\tan\theta}{Z_a} - j\frac{1}{Z_b \tan\theta}. \tag{12}$$

When Y_{ocsc} is equal to zero, OCSC-1 looks like that it is nonexistent at f_1 and f_2. For this reason, Z_a and Z_b should meet the following equation

$$Z_a = Z_b \tan^2\theta. \tag{13}$$

An additional consideration is that the two formulas can be used not only at f_1 but also at f_2. Therefore, θ should satisfy

$$u_1\theta = \theta + p\pi, \tag{14a}$$

$$u_1\theta = p\pi - \theta, \tag{14b}$$

$$\theta = \frac{p\pi}{u_1 - 1} \text{ or } \frac{p\pi}{u_1 + 1}, \tag{14c}$$

where p is a natural number. The characteristic parameters of OCSC-2 can be defined by the same way. In this paper, $u_1 = f_2/f_1$. However, for the admittance at f_3, OCSC stubs can change its imaginary part.

There is a temporary assumption that OCSC-2 doesn't exist, so $Y_{in3} = Y_{in2}$.

Stub-3 is a cascaded transmission line. The admittance at its left hand is expressed by (15). As is known to all, the impedance transformer function of the transmission line disappears when its characteristic impedance is equal to the impedance connected with it. This is the reason why Z_3 is fixed to Z_0 ($Z_0 = 1/Y_{in2}$ @ $f_1 = 1/Y_{in2}$ @ f_2).

Because the source impedance is a real-value impedance, the real part of Y_{in4} should be the reciprocal of the source impedance whereas the imaginary part should be eliminated by OCSC-1. According to the above constraint and (15), two equations can be established and they are (16) and (17). In this paper, $u_2 = f_3/f_1$. (18) derives from (16). Due to the periodicity of the tangent function, there is a series of solutions of θ_3. Choosing a solution with small value is beneficial to reducing the size of the circuit structure. Then, bring the known θ_3 and Z_3 into (17) to calculate B_4. (15)-(18) are shown at the bottom of this page.

The combination of (13) and (17) arrives at

$$Y_a = -\frac{B_4}{\tan(u_2\theta) - \tan^2\theta \cot(u_2\theta)}. \tag{19}$$

At the end, this paper investigates whether the existence of OCSC-2 is necessary. If OCSC-2 does not exit, $Y_{in2} = Y_{in3}$. If OCSC-2 exits, the relationship between Y_{in2} and Y_{in3} is expressed as

$$B_3 = B_2 - Y_d \cot(u_2\theta) + Y_c \tan(u_2\theta), \tag{20}$$

$$G_3 = G_2. \tag{21}$$

G_2 and B_2 may influence the parameters of stub-3 and OCSC-1 by (15)-(21). Z_a and Z_b must be controlled among 30 to 120 Ω, which makes sure the widths of OCSC-1 are moderate. There are two tables and a figure to show the variations of Z_a and Z_b with G_2 and B_2. The experimental condition of Table 1 is $u_1 = 2.5$, $u_2 = 2.2$, and $Z_c = 120$ Ω and the experimental condition of Table 2 is $u_1 = 2.5$, $u_2 = 2.2$, and $Z_c = 50$ Ω.
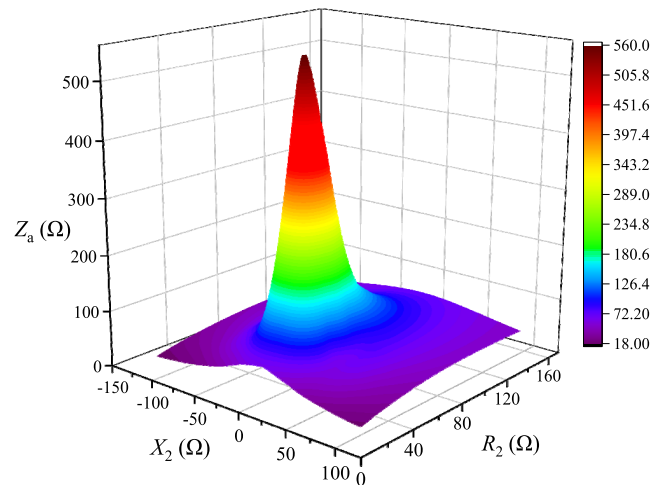

FIGURE 3. The influence of R_2 and X_2 on Z_a when OCSC-2 doesn't exit.

As shown in Fig. 3, Table 1, and Table 2, when X_2 is close to zero, the value of Z_a is too huge to realize. The conclusion is that X_2 is the decisive factor for the existence of OCSC-2. If X_2 is close to zero, designers should add OCSC-2 into their designs.

$$Y_{in4}\big|_{f_3} = \frac{Z_3 + jZ_{in3}\big|_{f_3} \tan u_2\theta_3}{Z_{in3}\big|_{f_3} Z_3 + jZ_3^2 \tan u_2\theta_3} = \frac{Z_0 + jZ_{in3}\big|_{f_3} \tan u_2\theta_3}{Z_{in3}\big|_{f_3} Z_0 + jZ_0^2 \tan u_2\theta_3} = G_4 + jB_4, \tag{15}$$

$$G_4 = \frac{G_3\left[1 + \tan^2(u_2\theta_3)\right]}{[1 - Z_0 B_3 \tan(u_2\theta_3)]^2 + [Z_0 G_3 \tan(u_2\theta_3)]^2} = \frac{1}{Z_0}, \tag{16}$$

$$B_4 = \frac{1}{Z_0}\frac{[1 - Z_0 B_3 \tan(u_2\theta_3)][Z_0 B_3 + \tan(u_2\theta_3)] - Z_0^2 G_3^2 \tan(u_2\theta_3)}{[1 - Z_0 B_3 \tan(u_2\theta_3)]^2 + [Z_0 G_3 \tan(u_2\theta_3)]^2} = Y_b \cot(u_2\theta) - Y_a \tan(u_2\theta), \tag{17}$$

$$\theta_3 = \frac{1}{u_2} \arctan\left[\frac{Z_0 B_3 \pm \sqrt{(Z_0 B_3)^2 - (1 - Z_0 G_3)(Z_0^2 B_3^2 + Z_0^2 G_3^2 - Z_0 G_3)}}{(Z_0^2 B_3^2 + Z_0^2 G_3^2 - Z_0 G_3)}\right]. \tag{18}$$

TABLE 1. The calculated impedances of ocsc-1 under different conditions ($B_2 < 0$).

Y_{in2}		Z_{in2}		Without OCSC-2		With OCSC-2	
G_2	B_2	R_2	X_2	Z_a	Z_b	Z_a'	Z_b'
0.005	-0.01	40.0	80.0	46.3	29.4	29.6	18.8
0.015	-0.01	46.2	30.8	129.2	82.1	59.2	37.6
0.025	-0.01	34.5	13.8	166.8	106.1	76.4	48.6

TABLE 2. The calculated impedances of ocsc-1 under different conditions ($B_2 > 0$).

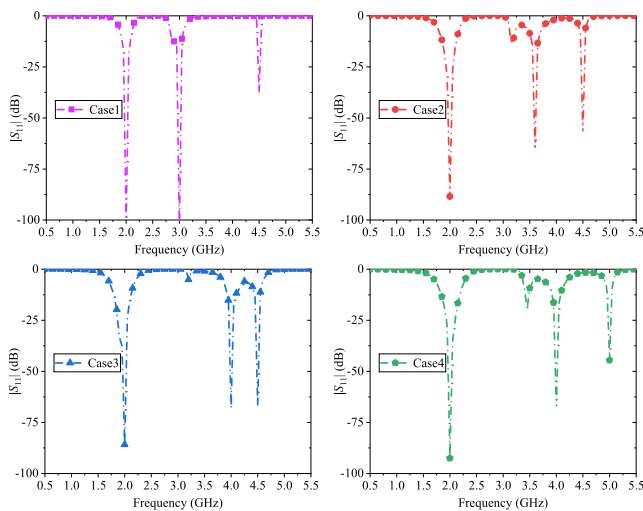| Y_{in2}		Z_{in2}		Without OCSC-2		With OCSC-2	
G_2	B_2	R_2	X_2	Z_a	Z_b	Z_a'	Z_b'
0.005	0.01	40.0	-80.0	46.2	29.4	30.0	19.1
0.015	0.01	46.2	-30.8	129.2	82.2	60.5	38.5
0.025	0.01	34.5	-13.8	166.8	106.1	78.1	49.7

FIGURE 4. The reflection coefficients of the TBITs in different cases.

It deserves to be mentioned that there are no strict limitations on Z_c. Designers can choose proper Z_c to alter X_2.

There are some cases used to show that the TBIT can transform frequency-dependent complex impedances to a real-value impedance. Conditions are listed in Table 3. The corresponding reflection coefficients are exhibited in Fig. 4.

TABLE 3. Operation frequencies in different cases.

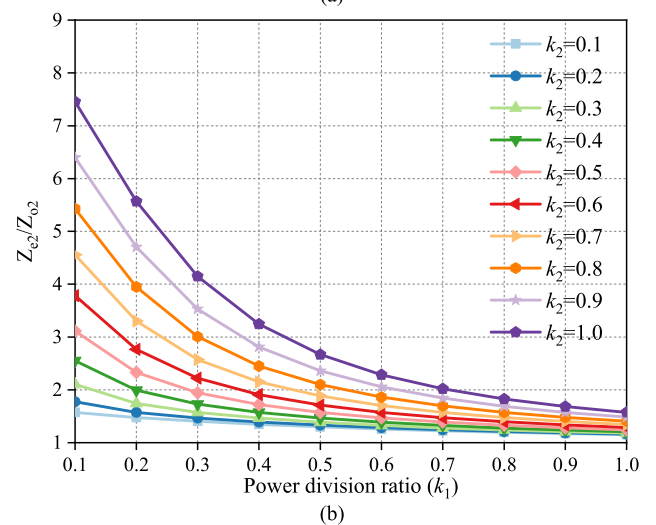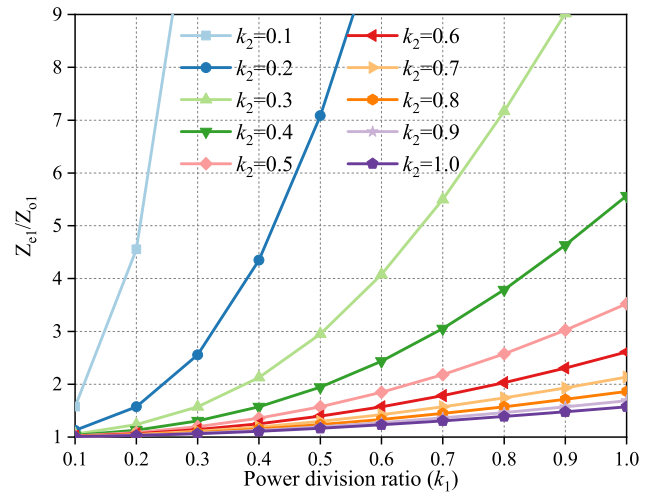| Cases	f_1 (GHz)	f_2 (GHz)	f_3 (GHz)	Conditions
Case-1	2.0	3.0	4.5	$Z_L@f_1$=30-10*j Ω,
Case-2	2.0	3.6	4.5	$Z_L@f_2$=40-20*j Ω,
Case-3	2.0	4.0	4.5	$Z_L@f_3$=50-30*j Ω,
Case-4	2.0	4.0	5.0	Z_S=50 Ω.

FIGURE 5. (a) The ratios of Z_{e1} and Z_{o1} with different power division ratios. (b) The ratios of Z_{e2} and Z_{o2} with different power division ratios.

Although the TBIT can transform frequency-dependent complex impedances to a real-value impedance, the proposed TTPD only uses it to complete the transformation between real-value impedances. In other words, X_L is zero. Hence, the related equations become compact.

B. TRI-BAND POWER DIVIDER

The previous part uses numerous equations to introduce a new TBIT which can transform frequency-dependent complex impedances to a real-value impedance. How to use this TBIT in PDs is the subject of this part. As exhibited in Fig. 1, the TTPD's terminal impedances are R_1, R_2, and R_3. At the junction, the impedances looking into two output paths are R_{2i} and R_{3i}, they are transformed from terminal impedances R_2 and R_3 by TBITs.

If the voltage at the junction is V_0, P_{2i} and P_{3i} can be expressed by (22) and (23), P_{2i} and P_{3i} refer to the power divided to two output paths, respectively. And the power
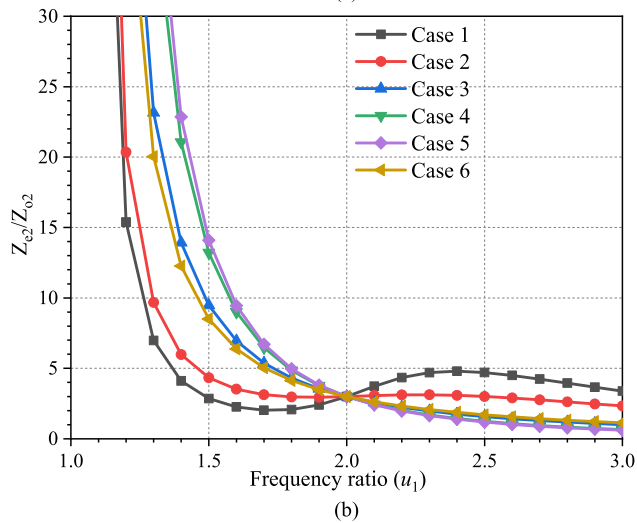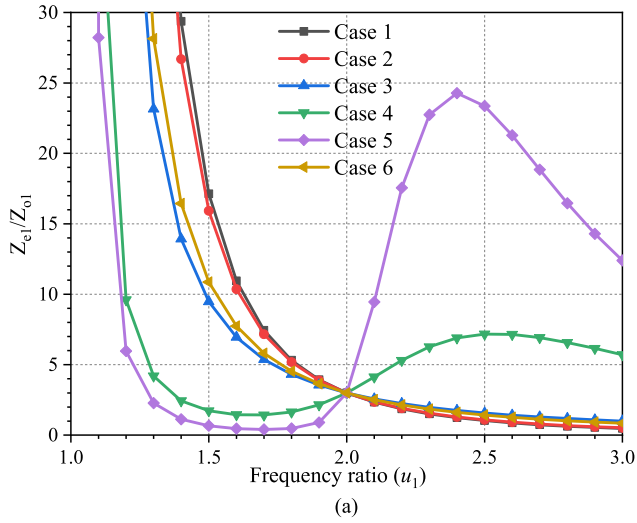
FIGURE 6. (a) The ratios of Z_{e1} and Z_{o1} in different cases. (b) The ratios of Z_{e2} and Z_{o2} in different cases.

FIGURE 7. The photography of the proposed power divider on the substrate of RO4350B.
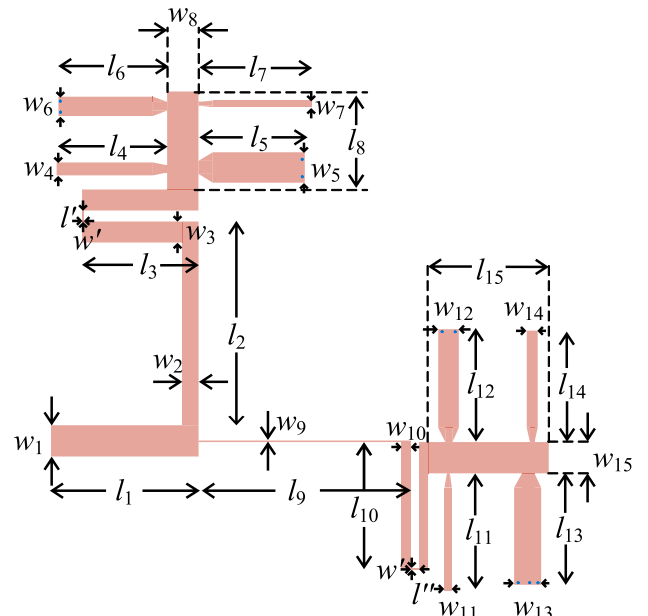
FIGURE 8. The dimension drawing of the proposed power divider.

TABLE 4. Variables in different cases.

Cases	k_1	k_2
Case-1	0.2	0.9
Case-2	0.3	0.8
Case-3	0.5	0.5
Case-4	0.8	0.3
Case-5	0.9	0.2
Case-6	0.6	0.7

division ratios k_i^2 are related to R_{2i} and R_{3i}

$$P_{2i} = \frac{V_0^2}{R_{2i}}, \tag{22}$$

$$P_{3i} = \frac{V_0^2}{R_{3i}}, \tag{23}$$

$$k_i^2 = \frac{P_{3i}}{P_{2i}} = \frac{R_{2i}}{R_{3i}}. \tag{24}$$

According to the theory of Kirchhoff Circuit Laws (KCL) and impedance matching, R_{2i} and R_{3i} must satisfy the following conditions to eliminate reflections. After rearranging (24) and (25), the relationships between R_{2i}, R_{3i} and k_i^2 can be described clearly. The power division ratios k_i^2 are important design goals, once k_i^2 and R_1 are set as two specific values, R_{2i} and R_{3i} are determined correspondingly. The design of the two TBITs regards R_2 and R_3 as the source impedances and regards R_{2i} and R_{3i} as the load impedances. Next, using (1)-(21) is able to complete the design of TBITs. Finally, the two TBITs make up the
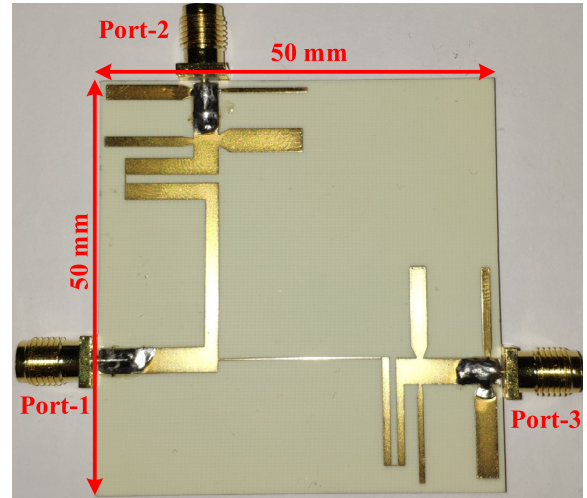
TTPD. In the following design, R_1, R_2, and R_3 are set to 50 Ω. Specially, when the TTPD needs to connect three terminals whose impedances' values are not 50 Ω, it is

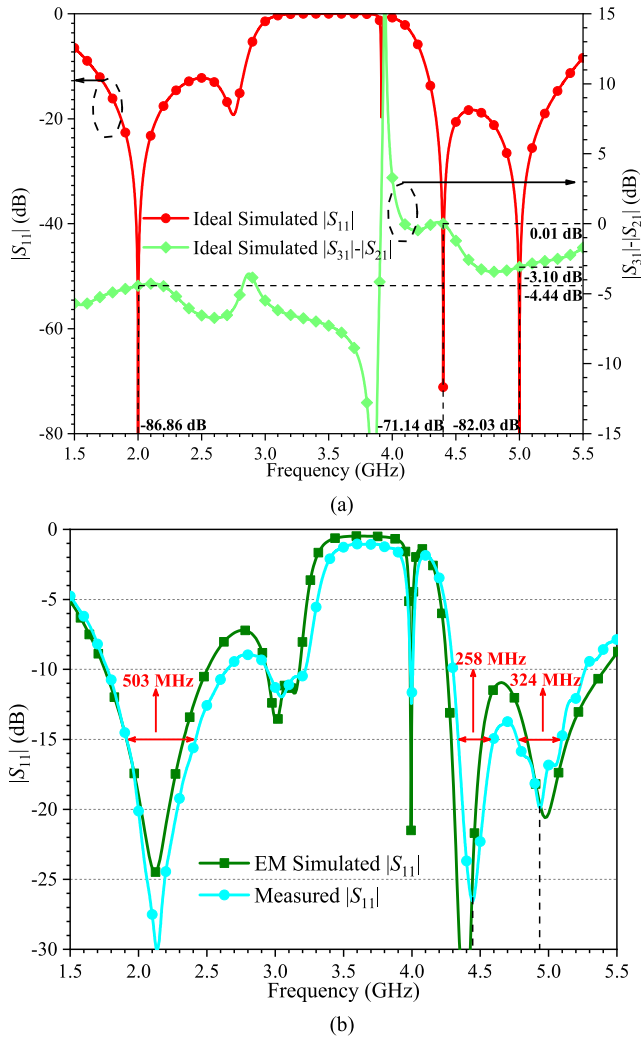**FIGURE 9.** (a) The ideal simulated results of $|S_{11}|$ and $|S_{31}| - |S_{21}|$. (b) The EM simulated and measured results of $|S_{11}|$.

TABLE 5. The design parameters of the proposed power divider.

Tri-band impedance transformer-1	
$Z_1, Z_3, Z_e, Z_o, Z_a, Z_b, Z_c, Z_d$	$\theta, \theta_1, \theta_2, \theta_3$
71.18Ω, 50.00Ω, 72.68Ω, 51.07Ω, 103.32Ω, 65.71Ω, 80.00Ω, 50.88Ω.	51.43°, 77.15°, 51.43°, 45.94°.
Tri-band impedance transformer-2	
$Z_1, Z_3, Z_e, Z_o, Z_a, Z_b, Z_c, Z_d$	$\theta, \theta_1, \theta_2, \theta_3$
169.47Ω, 50.00Ω, 114.52Ω, 67.25Ω, 85.82Ω, 54.58Ω, 100.00Ω, 63.60Ω.	51.43°, 77.15°, 51.43°, 48.00°.

$\theta, \theta_1, \theta_2$, and θ_3 are defined at 2.0 GHz.

useful too

$$R_1 = \frac{R_{2i}R_{3i}}{R_{2i} + R_{3i}}, \tag{25}$$

$$R_{2i} = R_1 \left(1 + k_i^2 \right), \tag{26}$$

$$R_{3i} = R_1 \left(1 + \frac{1}{k_i^2} \right). \tag{27}$$

TABLE 6. The physical dimensions (lengths) of the proposed power divider. (Units: mm.)

$l_1 = 15.50$	$l_2 = 21.44$	$l_3 = 12.24$	$l_4 = 11.61$	$l_5 = 11.17$
$l_6 = 11.42$	$l_7 = 11.86$	$l_8 = 10.32$	$l_9 = 22.30$	$l_{10} = 13.44$
$l_{11} = 12.33$	$l_{12} = 11.88$	$l_{13} = 11.73$	$l_{14} = 11.73$	$l_{15} = 12.68$
$l' = 1.16$	$l'' = 0.86$			

TABLE 7. The physical dimensions (widths) of the proposed power divider. (Units: mm.)

$w_1 = 3.29$	$w_2 = 1.74$	$w_3 = 2.21$	$w_4 = 1.36$	$w_5 = 3.20$
$w_6 = 2.03$	$w_7 = 0.71$	$w_8 = 3.29$	$w_9 = 0.16$	$w_{10} = 0.95$
$w_{11} = 0.78$	$w_{12} = 2.16$	$w_{13} = 2.84$	$w_{14} = 1.15$	$w_{15} = 3.29$
$w' = 0.10$				
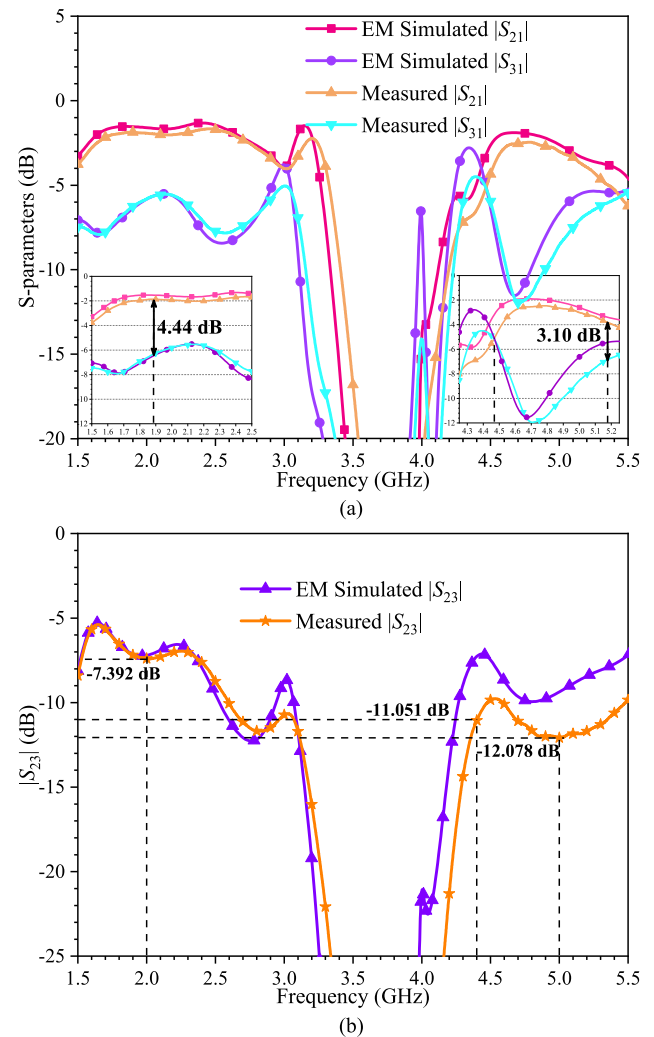
FIGURE 10. (a) The EM simulated and measured results of $|S_{21}|$ and $|S_{31}|$. (b) The EM simulated and measured results of $|S_{23}|$.

This work is mainly concerned with independent control-lable power division ratios. As is discussed, power division ratios influence R_{2i} and R_{3i}. As the load impedances of TBIT, R_{2i} and R_{3i} will influence the odd- and even-mode impedance of the coupled line. Fig. 5 and Fig. 6 show the variation

TABLE 8. The performance comparisons of some similar power dividers.

Refs.	Operation frequency	Central frequency (GHz)	FBW	CPDR	Size (mm²)
[22]	Dual-band	0.9/2.1	22.2% & 9.5%	No	52×39
[10]	Dual-band	2.4/3.8	16.3% & 10.3%	Yes	N/A
[14]	Dual-band	1.0/1.8	15.4% & 5.2%	Yes	N/A
[15]	Dual-band	0.9/2.0	33.9% & 7.7%	Yes	30×85*
[17]	Tri-band	1.0/1.3/3.3	9.7% & 8.1% & 3.3%	No	110×110
[30]	Tri-band	1.0/2.55/3.0	20.0% & 5.8% & 3.8%	No	37×41*
[29]	Tri-band	1.0/1.6/2.35	9.2% & 3.2% & 1.5%	Yes	70×150*
This work	Tri-band	2.0/4.4/5.0	23.2% & 5.8% & 6.6%	Yes	50×50

FBW: Fractional bandwidth ($|S_{11}| < $ -15 dB); CPDR: Controllable power division ratio; *: Estimated value.

of Z_{ej}/Z_{oj} with power division ratios ($j = 1, 2$). j is used to distinguish two output paths. Specially, these results are obtained under the condition of $u_1 = 2.2$. For the coupled line, the huger imbalance between Z_e and Z_o is, the smaller distance is. The advice is that the ratio of Z_{ej} and Z_{oj} should be within the range of 1.0 to 2.5.

C. DESIGN STEPS

There have been enough considerations on the selections of the parameters. On the basis of these works, design steps are listed as

1) According to the operation frequencies of the TTPD, frequency ratios u_1 and u_2 can be calculated.
2) Use (1)-(10) to determine the change range of k_i^2 within which the ratio of Z_e and Z_o is proper. Choose a couple of power division ratios for f_1 and f_2. The power division ratio k_3^2 at f_3 doesn't have an impact on Z_e and Z_o, so designers can choose it independently.
3) For given k_i^2, u_1, and u_2, use (4)-(5), (9)-(11), and (26)-(27) to determine the parameters in section-1. Depending on calculations or simulations, Y_{in2} @ f_3 can be obtained. Decide whether to add OCSC-2 into the design according to its value. If OCSC-2 is necessary, choose a proper Z_c to change Y_{in2} @ f_3 to Y_{in3} @ f_3. In OCSC-2, the value of Z_c is adjustable.
4) Search the remaining unknown parameters of the TBIT by computing (15)-(21).
5) Connect two TBITs in parallel form.

III. SIMULATED AND MEASURED RESULTS

In the light of the design steps, an ideal TTPD with independent controllable power division ratios at 2.0 GHz, 4.4 GHz, and 5.0 GHz is designed and simulated in ADS.

Power division ratios are -4.44 dB, 0.00 dB, and -3.10 dB. It is worth to mention that this design views 5.0 GHz as f_2 and views 4.4 GHz as f_3. By calculating (26) and (27), at f_1, f_2, and f_3, load impedances (Z_L in Fig. 2) of output path-1's TBIT are set to 68.00 Ω, 74.50 Ω, and 100.00 Ω respectively, and load impedances of the other output path's TBIT are set to 188.89 Ω, 152.04 Ω, 100.00 Ω. By a series of calculations, parameters listed in Table 5 can be determined. For validating the correctness, this TTPD is fabricated on the RO4350B substrate. This material's relative dielectric constant, thickness, and loss tangent are 3.48, 1.524 mm, and 0.0037. Fig. 7 and Fig. 8 are the photograph and dimension drawing of the fabricated TTPD, after a little optimization the physical dimensions are set to values exhibited by Table 6 and Table 7 in detail. Connections between actual microstrips make circuit parameters deviate from the ideal simulation. In order to reduce this negative impact, this design use trapezoid microstrips to link different parts. Some dimensions showed in Table 6 and Table 7 have covered lengths and widths of these trapezoid microstrips. The overall size of the TTPD is 50 × 50 mm² which is smaller than the similar design in [29].

Fig. 9(a) shows the ideal simulated results in ADS. It illustrates not only the input return loss but also the difference between two insertion loss coefficients. It shows a perfect agreement with the design goals. The electromagnetic (EM) simulator can link the theoretical design to the reality. EM simulated results are exhibited in Fig. 9(b). The measured results are shown in the same picture for comparison. The measured results show that the first band with $|S_{11}| \leq -15$ dB is from 1.914 GHz to 2.417 GHz and the fractional bandwidth is about 23.23%. The second band with $|S_{11}| \leq -15$ dB is from 4.340 GHz to 4.598 GHz and the

fractional bandwidth is about 5.77%. The third band with $|S_{11}| \leq -15$ dB covers 4.772 GHz to 5.096 GHz and the fractional bandwidth is approximately 6.57%.

Fig. 10(a) shows the variation trend of the power division ratios which is revealed by the amplitude imbalances of $|S_{21}|$ and $|S_{31}|$. At 1.891 GHz, 4.467 GHz, and 5.170 GHz, the values of $|S_{31}| - |S_{21}|$ are -4.44 dB, 0.00 dB, and -3.10 dB. It proves that this design achieves expected targets and the power division ratios of this TTPD are controllable. The shift of the center frequencies and the performance deterioration are due to the unavoidable machining error and the test error.

In addition, the curves used to describe the EM simulated and measured results of $|S_{23}|$ are drawn in Fig. 10(b). The curves reflect of the isolation between two output ports. Without any isolation resistor, this TTPD can obtain 7.392 dB, 11.051 dB, and 12.078 dB isolation at 2.0 GHz, 4.4 GHz, and 5.0 GHz.

IV. CONCLUSION

In general, a TTPD with independent controllable power division ratios at different frequencies is proposed. This design also includes a new TBIT. The theory and the design idea are shown by some detailed and computable mathematical formulas. Furthermore, there are simple and clear design steps in this paper. An ideal design example with power division ratios of -4.44 dB, 0.00 dB, and -3.10 dB at frequency points of 2.0 GHz, 4.4 GHz, and 5.0 GHz demonstrates that the theory mentioned in this paper is right. The corresponding experiments show that this TTPD have advantages of tri-band operation, independent controllable power division ratios, and enhanced bandwidths. Table 8 shows the comparisons with some previous power dividers. These advantages make it possible to use this TTPD as a feed network of array antennas. Active components such as Doherty power amplifiers can also use it.
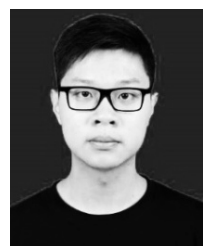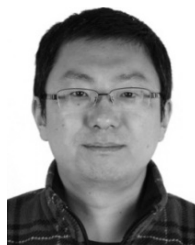
REFERENCES

[1] F. Wei, X. W. Shi, P. Y. Qin, and Y. J. Guo, "Compact UWB power divider with unequal distribution ratio," in *Proc. Int. Workshop Antenna Technol., Small Antennas, Novel EM Struct. Mater., Appl.*, Mar. 2014, pp. 297–299.

[2] T. Zhang, X. Wang, and W. Che, "A varactor based frequency-tunable power divider with unequal power dividing ratio," *IEEE Microw. Wireless Compon. Lett.*, vol. 26, no. 8, pp. 589–591, Aug. 2016.

[3] M. Chongcheawchamnan, S. Patisang, M. Krairiksh, and I. D. Robertson, "Tri-band Wilkinson power divider using a three-section transmission-line transformer," *IEEE Microw. Wireless Compon. Lett.*, vol. 16, no. 8, pp. 452–454, Aug. 2006.

[4] M.-J. Park, "Dual-band unequal power divider with simplified structure," *IET Microw., Antennas Propag.*, vol. 5, no. 15, pp. 1891–1896, Dec. 2011.

[5] M. Hayati, S.-A. Malakooti, and A. Abdipour, "A novel design of triple-band Gysel power divider," *IEEE Trans. Microw. Theory Techn.*, vol. 61, no. 10, pp. 3558–3567, Oct. 2013.

[6] B.-S. Wu, Y.-C. Lin, K.-H. Lin, and J.-D. Tseng, "Tri-band Wilkinson power divider for TD-LTE/3G/GPS systems," in *Proc. IEEE Int. Workshop Electromag.*, Aug. 2014, pp. 189–190.

[7] B. M. Abdelrahman, H. N. Ahmed, and A. I. Nashed, "A novel tri-band Wilkinson power divider for multiband wireless applications," *IEEE Microw. Wireless Compon. Lett.*, vol. 27, no. 10, pp. 891–893, Oct. 2017.

[8] F.-X. Liu, Y. Wang, X.-Y. Zhang, C.-H. Quan, and J.-C. Lee, "A size-reduced tri-band Gysel power divider with ultra-wideband harmonics suppression performance," *IEEE Access*, vol. 6, pp. 34198–34205, 2018.

[9] M. J. Park, "Two-section cascaded coupled line Wilkinson power divider for dual-band applications," *IEEE Microw. Wireless Compon. Lett.*, vol. 19, no. 4, pp. 188–190, Apr. 2009.

[10] Z. Lin and Q.-X. Chu, "A novel approach to the design of dual-band power divider with variable power dividing ratio based on coupled-lines," *Prog. Electromagn. Res.*, vol. 103, pp. 271–284, 2010.

[11] X. Tang and K. Mouthaan, "Compact dual-band power divider with single allpass coupled lines sections," *Electron. Lett.*, vol. 46, no. 10, pp. 688–689, May 2010.

[12] Y. Wu, Y. Liu, and Q. Xue, "An analytical approach for a novel coupled-line dual-band Wilkinson power divider," *IEEE Trans. Microw. Theory Techn.*, vol. 59, no. 2, pp. 286–294, Feb. 2011.

[13] W.-H. Chen, Y.-C. Liu, X. Li, Z.-H. Feng, and F. M. Ghannouchi, "Design of reduced-size unequal power divider for dual-band operation with coupled lines," *Electron. Lett.*, vol. 47, no. 1, pp. 59–60, Jan. 2011.

[14] B. Li, X. Wu, N. Yang, and W. Wu, "Dual-band equal/unequal Wilkinson power dividers based on coupled-line section with short-circuited stub," *Prog. Electromag. Res.*, vol. 111, pp. 163–178, 2011.

[15] Y. Liu, W. Chen, X. Li, and Z. Feng, "Design of compact dual-band power dividers with frequency-dependent division ratios based on multisection coupled line," *IEEE Compon., Packag., Manuf. Technol.*, vol. 3, no. 3, pp. 467–475, Mar. 2013.

[16] C.-W. Tang and Z.-Q. Hsieh, "Design of a planar dual-band power divider with arbitrary power division and a wide isolated frequency band," *IEEE Trans. Microw. Theory Techn.*, vol. 64, no. 2, pp. 486–492, Feb. 2016.

[17] H.-H. Chen and Y.-H. Pang, "A tri-band Wilkinson power divider utilizing coupled lines," in *Proc. IEEE Int. Symp. Antennas Propag.*, Jul. 2011, pp. 25–28.

[18] N. Gao, G. Wu, and Q. Tang, "Design of a novel compact dual-band Wilkinson power divider with wide frequency ratio," *IEEE Microw. Wireless Compon. Lett.*, vol. 24, no. 2, pp. 81–83, Feb. 2014.

[19] Y. C. Li, Q. Xue, and X. Y. Zhang, "Single- and dual-band power dividers integrated with bandpass filters," *IEEE Trans. Microw. Theory Techn.*, vol. 61, no. 1, pp. 69–76, Jan. 2013.

[20] F. Lin, Q.-X. Chu, Z. Gong, and Z. Lin, "Compact broadband Gysel power divider with arbitrary power-dividing ratio using microstrip/slotline phase inverter," *IEEE Trans. Microw. Theory Techn.*, vol. 60, no. 5, pp. 1226–1234, May 2012.

[21] W. Q. Liu, F. Wei, and X. W. Shi, "A compact tri-band power divider based on triple-mode resonator," *Prog. Electromagn. Res.*, vol. 138, pp. 283–291, Jun. 2013.

[22] H.-J. Zhou, H.-F. Wu, G.-Z. Lei, and Y.-Z. Ma, "Design of a compact tri-band power divider with unequal outputs," *Progr. Electromagn. Res. C*, vol. 41, pp. 255–265, 2013.

[23] C. Shao, Y. Li, and J.-X. Chen, "Compact dual-band microstrip filtering power divider using T-junction structure and quarter-wavelength SIR," *Electron. Lett.*, vol. 53, no. 6, pp. 434–436, Jan. 2017.

[24] K. Song, M. Fan, F. Zhang, Y. Zhu, and Y. Fan, "Compact triple-band power divider integrated bandpass-filtering response using short-circuited SIRs," *IEEE Trans. Compon., Packag., Manuf. Technol.*, vol. 7, no. 7, pp. 1144–1150, Jul. 2017.

[25] Y.-F. Bai, X.-H. Wang, C.-J. Gao, X.-W. Shi, and H.-J. Lin, "Compact dual-band power divider using non-uniform transmission line," *Electron. Lett.*, vol. 47, no. 3, pp. 188–190, Feb. 2011.

[26] A. Genc and R. Baktur, "Dual- and triple-band Wilkinson power dividers based on composite right- and left-handed transmission lines," *IEEE Trans. Compon., Packag., Manuf. Technol.*, vol. 1, no. 3, pp. 327–334, Mar. 2011.

[27] Z. Zhuang, Y. Wu, M. Kong, W. Wang, and Y. Liu, "Dual-band filtering balanced-to-unbalanced impedance-transforming power divider with high frequency ratio and arbitrary power division," *IEEE Access*, vol. 6, pp. 12710–12717, 2018.

[28] W. Zhang, Z. Ning, Y. Wu, C. Yu, S. Li, and Y. Liu, "Dual-band out-of-phase power divider with impedance transformation and wide frequency ratio," *IEEE Microw. Wireless Compon. Lett.*, vol. 25, no. 12, pp. 787–789, Dec. 2015.

[29] Y. Wu, Y. Guan, Z. Zhuang, W. Wang, and Y. Liu, "A novel tri-band T-junction impedance-transforming power divider with independent power division ratios," *PLoS ONE*, vol. 12, no. 6, Jun. 2017, Art. no. e0178956.

[30] Q. Chu, F. Lin, Z. Lin, and Z. Gong, "Novel design method of tri-band power divider," *IEEE Trans. Microw. Theory Techn.*, vol. 59, no. 9, pp. 2221–2226, Sep. 2011.

[31] R. K. Barik, T. S. L. Deep, and S. S. Karthikeyan, "An equal split triple-band Wilkinson power divider employing extended cross-shaped microstrip line," *Microw. Opt. Technol. Lett.*, vol. 60, no. 10, pp. 2488–2492, Oct. 2018.

[32] C. Monzon, "A small dual-frequency transformer in two sections," *IEEE Trans. Microw. Theory Techn.*, vol. 51, no. 4, pp. 1157–1161, Apr. 2003.

[33] M.-A. Maktoomi, A.-P. Yadav, M.-S. Hashmi, and F.-M. Ghannouchi, "Dual-frequency impedance matching networks based on two-section transmission line," *IET Microw., Antennas Propag.*, vol. 11, no. 10, pp. 1415–1423, Aug. 2017.

[34] Y. Wu, Y. Liu, and S. Li, "A compact Pi-structure dual band transformer," *Prog. Electromagn. Res.*, vol. 88, pp. 121–134, 2008.

[35] Y. Wu, Y. Liu, S. Li, C. Yu, and X. Liu, "A generalized dual-frequency transformer for two arbitrary complex frequency-dependent impedances," *IEEE Microw. Wireless Compon. Lett.*, vol. 19, no. 12, pp. 792–794, Dec. 2009.

[36] D. Rano, D. Banerjee, and M. S. Hashmi, "A miniaturized three-stage dual-frequency matching network," in *Proc. IEEE MTT-S Int. Microw. RF Conf.*, Dec. 2017, pp. 1–5.

[37] Y. Wu, W. Sun, S.-W. Leung, Y. Diao, and K.-H. Chan, "A novel compact dual-frequency coupled-line transformer with simple analytical design equations for frequency-dependent complex load impedance," *Prog. Electromagn. Res.*, vol. 134, pp. 47–62, Feb. 2013.

[38] X.-H. Wang, L. Zhang, Y. Xu, Y.-F. Bai, C. Liu, and X. Shi, "A tri-band impedance transformer using stubbed coupling line," *Prog. Electromagn. Res.*, vol. 141, pp. 33–45, Sep. 2013.

[39] M. A. Maktoomi, R. Gupta, M. H. Maktoomi, M. S. Hashmi, and F. M. Ghannouchi, "A genaralized multi-frequency impedance matching technique," in *Proc. 16th Medit. Microw. Symp.*, Nov. 2016, pp. 1–4.

[40] D. Banerjee, A. Saxena, and M. S. Hashmi, "A novel concept of virtual impedance for high frequency tri-band impedance matching networks," *IEEE Trans. Circuits Syst. II, Exp. Briefs*, vol. 65, no. 9, pp. 1184–1188, Sep. 2018.

[41] D. Banerjee, A. Saxena, and M. Hashmi, "A novel compact tri-band matching network utilizing two dual-band transformers at a common reference frequency," in *Proc. IEEE Asia–Pacific Microw. Conf.*, Nov. 2017, pp. 1080–1083.

[42] M. A. Maktoomi, M. S. Hashmi, A. P. Yadav, and V. Kumar, "A generic tri-band matching network," *IEEE Microw. Wireless Compon. Lett.*, vol. 26, no. 5, pp. 316–318, May 2016.

[43] D. M. Pozar, *Microwave Engineering*, 3rd ed. New York, NY, USA: Wiley, 2005.

NAN HU (SM'18) received the B.E. degree in electronic engineering from the Chengdu University of Information Technology, Chengdu, China, in 2001. Since 2001, he has been the CTO of A-INFO Inc. (www.ainfoinc.com). His research interests include ultra wideband antennas, antenna arrays, transmit arrays, reflectar-rays, metasurface, metamaterial, EBG structures, RF/microwave and mm-wave components, and waveguide components.

Mr. Hu is a Senior Member of the Chinese Institute of Electronics (CIE) and a member of ACES. He has served as a member of the Technical Committee on Antenna Measurements of IEEE AP-S, in 2019, and a Committee Member of Antenna Branch of CIE. He has served as the Session Chair of ACES-China 2018. He has served on the editorial/review boards of several journals and conferences. Since 2014, he has been a Reviewer of some journals, including the IEEE T-AP, ACES Journal and Conference, the *Journal of Electromagnetic Waves and Applications*, the *IET Microwaves, Antennas & Propagation*, and the *IET Electronics Letters*.

WENQING XIE received the B.S. degree from Beijing Normal University, in 2002, and the M.S. degree from the Chinese Academy of Sciences, in 2005. Since 2016, he has been the Marketing Manager of A-INFO Inc. (www.ainfoinc.com). His research interests include ultra wideband antennas, design and application of microwave, millimeter-wave, and terahertz-wave antennas, 5G antenna and RF technology, 5G communication antenna and measurement, design and application of RF devices and systems, and material testing. He is a Senior Member of the Chinese Institute of Electronics and a member of ACES.

WEIMIN WANG received the B.S. degree in communication engineering, the M.S. degree in electromagnetic field and microwave technology, and the Ph.D. degree in electronic science and technology from the Beijing University of Posts and Telecommunications (BUPT), Beijing, China, in 1999, 2004, and 2014, respectively. In 2014, she joined BUPT, where she is currently an Associate Professor with the School of Electronic Engineering. Her research interests include electromagnetic field, antennas, and MIMO OTA measurement.

YUHAO YANG received the B.Eng. degree in communication engineering from the Xi'an University of Science and Technology, Xi'an, China, in 2018. He is currently pursuing the M.S. degree with the Beijing University of Posts and Telecommunications (BUPT), Beijing, China.

In 2018, he started his research as a graduate at BUPT. His research interests include power amplifiers, active integrated antennas, and multi-band impedance transformers.

YONGLE WU (M'12–SM'15) received the B.Eng. degree in communication engineering and the Ph.D. degree in electronic engineering from the Beijing University of Posts and Telecommunications (BUPT), Beijing, China, in 2006 and 2011, respectively.

In 2010, he was a Research Assistant with the City University of Hong Kong, Hong Kong. In 2011, he joined BUPT, where he is currently a Full Professor with the School of Electronic Engineering. His research interests include microwave components, circuits, antennas, and wireless system design.

• • •